

# EB-gMCR: ENERGY-BASED GENERATIVE MODELING FOR SIGNAL UNMIXING AND MULTIVARIATE CURVE RESOLUTION

**Yu-Tang Chang   Shih-Fang Chen**

Department of Biomechatronics Engineering  
National Taiwan University  
{b05611038, sfchen}@ntu.edu.tw

## ABSTRACT

Signal unmixing analysis decomposes data into basic patterns and is widely applied in chemical and biological research. Multivariate curve resolution (MCR), a branch of signal unmixing, separates mixed chemical signals into base patterns (components) and their concentrations, playing a key role in understanding composition. Classical MCR is typically framed as matrix factorization (MF) and requires a user-specified component count, usually unknown in real data. As dataset size or component count increases, the scalability and reliability of MF-based MCR face significant challenges. This study reformulates MCR as a generative process (gMCR), and introduces an energy-based deep learning solver, EB-gMCR, that automatically discovers the smallest component set able to reconstruct the data faithfully. EB-gMCR starts from a large candidate pool (e.g., 1024 spectra) and employs a differentiable gating network to retain only active components while estimating their concentrations. On noisy synthetic datasets containing up to 256 latent sources, EB-gMCR maintained  $R^2 \geq 0.98$  and recovered the component count within 5% of the ground truth; at lower noise it achieved  $R^2 \geq 0.99$  with near exact component estimation. Additional chemical priors, such as non-negativity or nonlinear mixing, enter as simple plug-in functions, enabling adaptation to other instruments or domains without altering the core learning process. By uniting high-capacity generative modeling and hard component selection, EB-gMCR offers a practical route to large-scale signal unmixing analysis, including chemical library-driven scenarios. The source code is available at [https://github.com/b05611038/ebgmcr\\_solver](https://github.com/b05611038/ebgmcr_solver).

## 1 INTRODUCTION

Multivariate curve resolution (MCR) is a signal unmixing technique commonly applied to chemical data, such as optical or mass spectra (de Juan & Tauler, 2021). The core concept involves treating chemical data ( $\mathbf{D}$ ) as a mixture of signals from multiple unknown and independent source patterns. One primary goal of MCR is to obtain these patterns ( $\mathbf{S}$ ) and their concentrations ( $\mathbf{C}$ , Eq. 1). Usually, the formulation of MCR includes a noise term ( $\mathbf{E}$ ) to represent signals introduced by chemical instruments. If a separated pattern closely approximates an actual source chemical pattern, it is possible to identify the chemical composition of the tested sample. Although MCR is conceptually intuitive, various practical difficulties arise in real-world applications. For instance, the types and number of mixed patterns are often unknown. The solution space becomes infinite unless additional constraints are imposed when solving the MCR equation.

$$\mathbf{D} = \mathbf{CS} + \mathbf{E} \tag{1}$$

MCR solvers can generally be divided into two categories: iterative and non-iterative. Non-iterative solvers find the solution by introducing suitable constraints to satisfy the full-rank condition, then solving the system of equations using classical matrix factorization methods in linear algebra. Constraints may be imposed on both the pattern and concentration matrices, primarily determined by

the chemical properties of the data. One commonly used constraint is retaining maximum information and imposing orthogonality on the pattern matrix, i.e. applying principal components for MCR solutions method (Lawton & Sylvestre, 1971), evolving factor analysis (EFA) (Keller & Massart, 1991), etc. Because some applications cannot formulate matrices that meet the full-rank requirement, iterative solvers are often viewed as a more general option for real-world problems. Iterative solvers compute solutions using a convex objective function, including Parallel Factor Analysis 2 (PARAFAC2) (Harshman, 1972), MCR-alternating least squares (ALS) (Tauler et al., 1995), etc. Although both iterative and non-iterative solvers can achieve satisfactory signal separation, their performance degrades under measurement noise and the numerical instability of large linear systems. Specifically, removing certain rows from the data matrix often prevents the estimated pattern and concentration matrices from remaining close to those derived from the full data matrix, even if both subsets originate from the same data acquisition process. This instability has led to a practical concern: can the calculated chemical components be readily used when a new dataset is collected? Alternatively, if candidate components are known based on prior chemical knowledge, is it possible to incorporate them into the MCR solver? For instance, (Barcaru et al., 2017) parsed GC-MS spectra using an existing mass spectrum library, and (Heinecke et al., 2021) analyzed metabolites by incorporating prior information from NMR signals.

Another practical concern in existing MCR solvers lies in their limited ability to honor basic chemical priors such as non-negativity in spectral data. Even a minor new constraint often requires a fresh solver because the task is framed as a fixed linear system. To align MCR more naturally with domain knowledge, we introduce generative MCR (gMCR) and—built on top of it—the energy-based solver EB-gMCR. Our contributions are fourfold:

- **EB-gMCR solver.** An energy-based generative solver that starts from an oversized component pool and uses the learnable gate **EB-select** to retain only the components needed for accurate reconstruction of mixed spectra.
- **Functional learning formulation of MCR.** The multicomponent resolution task is reformulated as learning a generating function via mini-batch optimization, avoiding repeated global matrix factorizations.
- **High-capacity yet compact solutions.** A selection energy objective combined with a non-duplicated component constraint lets the solver examine pools above 100 candidates—about ten times the scale of typical practice—yet still converge to models using less components.
- **Chemistry oriented plug-in priors.** Domain knowledge such as concentration normalization or non-negativity constraints enters through simple plug-in operators added to the model forward computation, so chemists can tailor the solver to new datasets without re-designing the core algorithm.

The study validates these ideas on all-positive, mixed spectral datasets, showing that EB-gMCR achieves high reconstruction accuracy while activating the fewest necessary components.

## 2 GENERATIVE MULTIVARIATE CURVE RESOLUTION (gMCR)

Revisiting the MCR problem setup, it represents mixed signals (data) as a linear combination of unknown components, where  $N \in \mathbb{N}$ . Typically, specifying a very large number of components (for example, more than a thousand) is impractical when both concentration and component matrices are unknown. However, if no prior assumption is made about potential chemical components, the number of components must be set high enough to ensure a sufficiently comprehensive solution space. Although using a large number of components is not common in traditional MCR solvers, searching for and combining both known and unknown patterns aligns more closely with the core idea of the original MCR problem. Consequently, the gMCR framework reformulates the MCR equation as a data generating function describing the mixing of chemical patterns, providing a dual representation: a generative view of the classical MCR problem (Eq. 2; Fig. 1) In this formulation,  $\delta$  is an indicator function for candidate patterns that participate in the mixing process, and  $\Phi$  is an aggregation function for these patterns. The nature of this aggregation depends on the instrument; for instance, in mass spectrometry it can be treated as simple addition. Furthermore, because each component’s indicator function is considered independent in the chemical signal mixing, the resulting generation

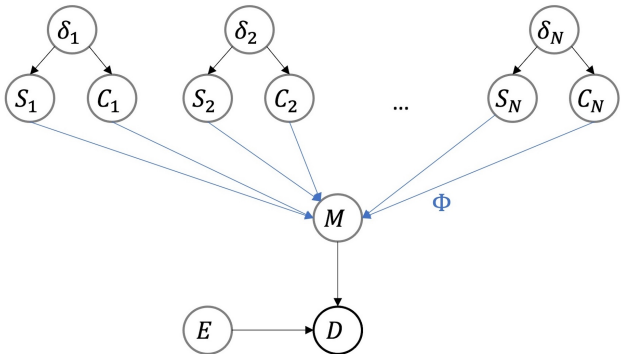


Figure 1: Graphical model of multivariate curve resolution (gMCR). Only the black node (representing the data  $\mathbf{D}$ ) is an observed variable, whereas the other gray nodes are hidden variables.

process approximating the true data generation process satisfies an intuitive incremental property (Eq. 3), where  $D_1$  denotes the generation process for a single component.

$$\mathbf{D}(\omega) = \Phi(\{\delta_i(\omega), \mathbf{C}_i(\omega), \mathbf{S}_i(\omega)\}_{i=1}^N) + \mathbf{E}(\omega) \quad (2)$$

$$\mathbf{D}_{i+j}(\omega) \approx \mathbf{D}_i(\omega) + \mathbf{D}_j(\omega) \quad (3)$$

The gMCR framework provides flexibility for incorporating prior knowledge of chemical signals and is solved by modeling the sampling function (paths) in a graphical model. In this sampling function modeling approach, all known mathematical descriptions of data generation can be expressed directly. For instance, in a GC-MS spectrum, peaks can be generated by mapping mass patterns onto a Gaussian distribution, parameterized by center time (mean shift) and peak width (small variance). If the modeled sample function closely approximates the true one, it can be reused whenever the data generation process remains unchanged. A key difference from conventional MCR methods is that gMCR does not force the solver to enforce constraints (such as orthogonality) that real components may fail to satisfy. Moreover, data size no longer drives a strict full-rank requirement; it simply sets the sampling duration of the generative process. This flexibility keeps gMCR practical even for extremely large datasets. Whereas traditional MCR hits memory limits once a data matrix grows to millions or billions of rows, gMCR sidesteps the barrier by computing in mini-batches, a strategy common in modern deep learning (DL) practice.

### 3 ENERGY-BASED DEEP GENERATIVE MODELING FOR gMCR (EB-gMCR)

The proposed EB-gMCR solver applies a probabilistic inference to approximate the sample function using parametric DL models. The primary focus here is to establish a flexible framework that aligns with practical chemical knowledge, rather than to develop a specific DL model. Section 3.1 reviews constraints derived from chemical knowledge; 3.2 presents EB-select module designed for modeling indicator function in gMCR; 3.3 details the core learning algorithm; finally, 3.4 describes termination criteria and checkpointing design of the EB-gMCR solver.

#### 3.1 HOW EBG-MCR INCORPORATES CONSTITUTIVE CHEMICAL CONSTRAINTS

In addressing chemical MCR tasks, certain mathematical properties must be included in the concentration and component matrices to reflect the prior knowledge associated with the analyzed data. Common properties considered in MCR solvers include “ambiguity of components” and “non-negativity of concentrations,” among others. Moreover, depending on the chemical instrumentation, “sparse components” and “non-negative components” may also be relevant. Because EBg-MCR explicitly models the entire data generation process with parametric models, some common constraints

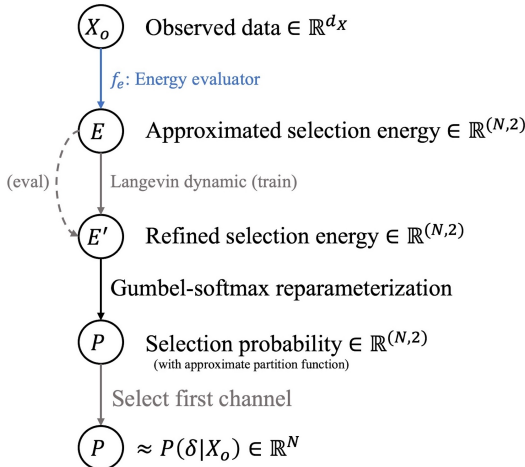


Figure 2: Energy-based adaptive selection (EB-select) module that simulates a hard selection process using variational inference and reparameterization tricks.

can be applied directly to the data generating function through unary function mappings. For example, to enforce “non-negativity of concentrations,” the concentration matrix can pass through an absolute operator or a rectified linear unit (ReLU) function to ensure that all outputs are non-negative. Constraints not represented by unary functions are handled in the core module of the EBg-MCR solver. Among these remaining constraints, two categories are particularly noteworthy: “sparsity” and “ambiguity of components.” Both require comparisons across multiple elements, so they cannot simply be imposed on the data-generation function.

### 3.2 ENERGY-BASED ADAPTIVE SELECTION MODULE FOR HANDLING MATRICES SPARSITY

A key distinction between gMCR and conventional MCR is the explicit modeling of the component appearance indicator  $\delta$ . The result of  $\delta$  is expected to form a sparse matrix, particularly in over-parameterized settings ( $N \gg N_{\text{true}}$ ). This scenario often arises if the chosen component candidates originate from an extensive chemical data library. In many chemical data types, such as mass spectra, zero values do not merely represent small magnitudes; instead, they signify that the corresponding feature is not selected. Conversely, any nonzero value in  $\delta$  indicates that the component has been adopted. In the context of a mass spectrum, a positive value implies a detected mass. It is intuitive to model the selection process using a gate-like function (e.g., a Sigmoid function). However, purely soft decision mechanisms may fail to block unselected elements completely, which can lead to the propagation of erroneous information in iterative solvers. Therefore, to enforce a “hard” decision, an energy-based adaptive selection module (EB-select) is introduced as a plugin whenever such a strict selection process is needed in the sample function (Fig. 2).

EB-select approximates the hard selection process by means of an energy evaluator that outputs select and non-select energies (Eq. 4). Because each spectrum  $X$  is observed only once,  $P(X)$  is treated as a Dirac delta centered at  $X_0$ . Under this deterministic prior, the marginal  $P(X)$  collapses to the conditional  $P(\delta|X_0)$  and is modeled by the EB-select energy function. The dimensionality of the resulting energy tensor equals the number of gating decisions; each decision supplies two energies, one for the select state and one for the reject state. These energies are converted to selection probabilities via the Gumbel-softmax reparameterization trick (Jang et al., 2016; Maddison et al., 2016). Intuitively, EB-select measures the selection probability of each component from observed data and produces a sparse selection matrix, denoting component usage for more accurate reconstruction (Eq. 5). The differentiable Gumbel-softmax layer allows gradients to propagate through this hard selection mechanism, enabling optimization of EB-select parameters via back-propagation. The temperature  $\tau$  of Gumbel-softmax trick gradually decreases during learning process to ensure convergence of the hard selection of EB-select.

$$\begin{aligned}
P(\delta) &= \int P(\delta, \mathbf{X}) d\mathbf{X} = \int P(\delta | \mathbf{X}) P(\mathbf{X}) d\mathbf{X} \\
&= \int P(\delta | \mathbf{X}) \delta_{\text{Dirac}}(\mathbf{X} - \mathbf{X}_0) d\mathbf{X} = P(\delta | \mathbf{X}_0)
\end{aligned} \tag{4}$$

$$f_e: \mathbf{X} \rightarrow [0, 1]^N, \quad f_e(\mathbf{X}) \approx \mathbb{E}[\delta | \mathbf{X}_0] \tag{5}$$

One might ask whether the module must be an “energy” evaluator, since it could also be regarded as a logit-based selector that reproduces the entire selection process. This design describes the EB-select module in its evaluation mode. However, in the training mode, EB-select refines its evaluated energy using Langevin dynamics (LD), a Markov chain Monte Carlo (MCMC)-like variant suitable for gradient-based optimization (Eq. 6). In this notation,  $t$  represents the step in LD, and  $\epsilon$  is the scale of LD noise. The stochastic gradient Langevin dynamic (SGLD) formula is rewritten in an approximate form (Eq. 7) (Welling & Teh, 2011) to enable parallel computation and prevent nested loops, where  $T$  is the total number of SGLD samples. In essence, the EB-select module constructs a local energy surface that depends only on the selection process, allowing additional manipulations on this local energy surface. The main advantage of applying SGLD is its exploratory effect, which yields a more generalizable selection energy evaluator whose select and non-select probabilities closely approximate the true indicator function in the data-generation process. To remain consistent with classical energy-based modeling, the selection energy must be bounded and kept it near a low-energy state. Accordingly, the overall loss includes an additional regularizer,  $\|\mathbf{E}_s \mathbf{e}\|_2^2$ , that penalizes the total selection energy and prevents it from drifting away from the minimal-energy configuration.

$$e_{t+1}^{(i)} = e_t^{(i)} - \frac{\epsilon}{2} \nabla_e E_{f_e}(e_t^{(i)}) + \sqrt{\epsilon} \eta_t^{(i)}, \quad i = 1, \dots, T \tag{6}$$

$$e' = e - \frac{T\epsilon}{2} \nabla_e E_{f_e}(e) + \sqrt{T\epsilon} \eta \tag{7}$$

### 3.3 ENERGY-BASED GENERATIVE MULTIVARIATE CURVE RESOLUTION (EB-gMCR) SOLVER

Although the formulation of gMCR differs from the MCR, its primary goals, acquiring the components and their concentrations, remain the same. Aside from modeling the indicator function, the sample functions for components  $f_s$  and for their concentrations  $f_c$  must still be constructed. To align with classical formulation (Eq. 1), the default version of  $f_s$  is defined as a threshold-based retrieval from a set of learnable component vectors  $\mathbf{s}_i \in \mathbb{R}^d$  (Eq. 8), where a component is included if its associated probability exceeds a threshold  $\tau$ , which is set close to 1 in practice. The default version of  $f_c$  is a vector-valued function, possibly parameterized by a neural network (NN), that directly evaluates concentration from the observed data (Eq. 9). In practice, users can extend these two sample functions by incorporating additional chemical knowledge. Finally, the data-generation process modeled in EB-gMCR reproduces the assumptions of the gMCR problem (Eq. 2).

$$f_s(f_e(X)) = \{\mathbf{s}_i | \delta_i = 1\}, \quad \text{where } \delta_i = \mathbb{I}(f_e(X_i) \geq \tau) \tag{8}$$

$$f_c: \mathcal{X} \rightarrow \mathbb{R}^N \tag{9}$$

With explicit access to  $f_s$  and its codomain, the crucial property of “component ambiguity” can be incorporated into the EB-gMCR’s learning process. Because the EB-gMCR solver is intended for over-parameterized conditions, duplicate components are not allowed in the final solution. Inspired by kernel-based measures for feature independence (e.g., the Hilbert-Schmidt independence criterion (HSIC) (Gretton et al., 2005) the dissimilarity among stored components can be evaluated in a reproducing kernel Hilbert space (RKHS). Specifically, the off-diagonal entries of the kernel matrix, generated by pairwise evaluation of the components, serve as a penalty (regularization term) to promote dissimilar components (Eq. 10). In this formulation,  $K$  is unspecified but must fulfill the

definition of a valid kernel function (with the semi-positive definite property). The default choice in the EB-gMCR is the radial basis function (RBF) kernel. In addition, component ambiguity helps the EB-select module construct a smoother energy surface that identifies fewer, yet more effective components for data reconstruction.

$$\mathcal{R}(X) = \sum_{\substack{i,j \in \mathcal{I}_X \\ i < j}} K(\mathbf{s}_i, \mathbf{s}_j), \quad \text{where } \mathcal{I}_X = \{i \mid f_e(X)_i \geq \tau\} \quad (10)$$

Although the HSIC regularizer discourages duplicate patterns, heavy over-parameterization introduces a second risk: a single ground-truth component can be represented by a linear combination of several learned patterns, thereby inflating the effective component count. To steer EB-gMCR toward the smallest feasible set, the solver activates an additional Lagrange multiplier term  $\lambda$  once the reconstruction error falls below a preset threshold (normalized mean square error smaller than 0.005). This term assigns a dynamic weight  $\lambda$  to a component usage cost  $C(X)$  (Eq. 11). Minimizing  $\lambda \cdot C(X)$  alongside the HSIC penalty drives the solver to retain only those non-redundant components that are strictly required to solve the MCR problem.

$$C(X) \equiv \frac{\sum f_e(X)}{N} \quad (11)$$

Finally, by explicitly defining all parametric functions in the EB-gMCR solver, one can approximate gMCR by enforcing that generated data remain close to the true data. Under the assumption that the background noise in gMCR is Gaussian (Eq. 12, replacing  $E(\omega)$  with a zero-mean Gaussian of variance  $\sigma^2$ ), the negative log-likelihood of  $X$  given the model parameters is proportional to the MSE (Eq. 13) (LeCun et al., 2006). Minimizing this MSE aligns the optimized parametric functions in the EB-gMCR solver with the underlying Gaussian data generation process. EB-gMCR can also be seen as an energy-based model, where the energy is  $\frac{1}{2\sigma^2} \|X - X_g\|^2$  plus regularizers (EB-select and component ambiguity). Under the noisy Gaussian assumption, no explicit partition function is necessary because the Gaussian likelihood is already normalized in closed form. Consequently, EB-gMCR does not require score matching to train the top-level (data generation) model. Although the solver can optionally include variational inference by treating the parametric functions in a fully Bayesian manner, the standard EB-based solver simply minimizes the MSE plus the aforementioned regularizations as a maximum-likelihood objective (Eq. 14). Finally, EB-gMCR can be solved via gradient-based frameworks such as PyTorch or TensorFlow.

$$X_g = \Phi(f_e, f_s, f_c) + \varepsilon, \quad \varepsilon \sim \mathcal{N}(0, \sigma^2 I) \quad (12)$$

$$-\log p(X \mid f_e, f_s, f_c) \propto \|X - X_g\|^2 \quad (13)$$

$$\mathcal{L}_{\text{EB-gMCR}} = \|X_o - X_g\|^2 + \lambda \cdot C(X_o) + \lambda_{\text{se}} \|E_{f_e}\|_2^2 + \lambda_{\text{amb}} \mathcal{R}(X_o) \quad (14)$$

### 3.4 EB-GMCR SOLVER AND MINIMUM COMPONENT CHECKPOINTING

traditional MCR workflows start with a small latent component set ( $N < 10$ ), enlarge  $N$ , and resolve (Eq. 1) at every step (Smith et al., 2019). EB-gMCR reverses the schedule: it launches from an intentionally oversized pool ( $N \gg 10$ ) and prunes away redundant components during training. The EB-select regularizer penalizes idle components, steering the solver to reproduce the observed data  $X_o$  with the fewest active components. Synthetic trials uncovered a characteristic trajectory. At first, both the active component count and the selection energy decrease. As the selection energy keeps falling, the active component count rises again and oscillates until the energy reaches its minimum. Reconstructions degrade when the active-component count dips below the ground-truth value, but accuracy returns once enough components reactivate. Importantly, reconstructions obtained while the selection energy is still far from its minimum are already as accurate as those at convergence. EB-gMCR exploits this behavior through **minimum component checkpointing**:

- **User-defined target band.** A reconstruction is considered eligible when its coefficient of determination falls inside the user-specified band (e.g.,  $0.975 \leq R^2 \leq 0.980$ ).
- **Single rolling checkpoint.** Whenever the current generating function satisfies the target band, the solver compares its active component count with that of the checkpoint already on disk. The checkpoint is replaced only if the new generating function uses fewer components, ensuring that at most one model—the most parsimonious acceptable one—is retained.
- **Termination.** Optimization stops once (i) the EB-select energy drops below the threshold  $\|E\|_2^2 < \sigma \|E_{init}\|_2^2$ , with  $\sigma = 0.25$  — a value lower enough to entering oscillatory phase based on preliminary test and (ii) the active-component count has entered a sustained oscillatory phase.

The result is a generator that meets the desired reconstruction accuracy while activating as few components as possible. The full optimization loop is summarized in **Algorithm 1**.

---

**Algorithm 1** EB-gMCR Solver: Training and Checkpointing Loop

---

**Inputs:** Observed data  $D_o$ , Components  $f_s$ , EB-select  $f_e$ , Concentration predictor  $f_c$

**Hyperparameters:** AdamW( $\eta=0.0005$ ,  $(\beta_1, \beta_2)=(0.9, 0.999)$ , weight\_decay= 0.001)

$\tau_0 = 1.0$ ,  $\tau_{\min} = 0.4$ ,  $t_{\text{eval}} = 0.01$ ,  $\lambda = 0$ ,  $\lambda_{\text{se}} = \lambda_{\text{amb}} = 1.0$

bands =  $[(0.97, 0.975), (0.975, 0.98), \dots, (0.995, 1.1)]$ , batch = 64

```

1: best[bands]  $\leftarrow \emptyset \forall$  bands
2:  $E_- \leftarrow f_E(D_o; \tau_0)^2$ 
3:  $E_{\text{init}} \leftarrow \text{mean}(E_-)$ 
4:  $E^* \leftarrow 0.25 \times E_{\text{init}}$ 
5: for each epoch do
6:   for minibatch  $B \sim \text{shuffled}(D_o)$  do
7:     # start of model forward:
8:      $\delta, E \leftarrow f_E(D; \tau), C \leftarrow f_C(D); S \leftarrow f_s$ 
9:      $D = \mathcal{T}(S \circ C)$  ▷ Reconstructed data
10:    # end of model forward:
11:     $\mathcal{R}_K \leftarrow \sum_{i < j, i, j \in \mathcal{I}} K(s_i, s_j), i \in \{i \mid E_i > 0\}$  ▷ Eq. 10
12:     $\mathcal{C}(S) \leftarrow \sum f_E(S)$  ▷ Eq. 11
13:     $\mathcal{L} \leftarrow \|D_o - D\|^2 + \lambda \cdot \mathcal{C}(S) + \lambda_{\text{se}} \|E\|^2 + \lambda_{\text{amb}} \mathcal{R}_K$  ▷ Eq. 14
14:    Backprop  $\leftarrow \text{AdamW}(\mathcal{L})$ 
15:     $\tau \leftarrow \max(\tau_{\min}, 0.999 \cdot \tau)$ 
16:   end for
17:   # ———— evaluate ————
18:    $\delta_{\text{all}}, E_{\text{all}} \leftarrow f_e(D_o, \tau_{\text{eval}}).detach(); C_{\text{all}}, D_{\text{all}} \leftarrow f_C(D_o).detach()$ 
19:    $D_{\text{all}} = \mathcal{T}(S_{\text{all}} \circ C_{\text{all}}); \text{metrics} = \{R^2, \text{MSE}, \text{nMSE}, \mathcal{L}, \text{usage}\}$ 
20:   for  $(lo, hi)$  in bands do
21:     if  $1 \leq R^2 < hi$  and best $[(lo, hi)].\text{usage} == \emptyset$  or  $\mathcal{C}(f_C) < \text{best}[(lo, hi)].\text{usage}$ 
22:       then
23:         best $[(lo, hi)] \leftarrow \{\text{state} = \text{copystate}(f_e, f_s, f_c), \text{usage} = \mathcal{C}(f_c)\}$ 
24:       end if
25:   end for
26:    $\lambda = 0.95 + 0.05 / (\text{MSE} \cdot \mathcal{C}(f_c))$ 
27:   until  $\text{mean}(\|E_{\text{all}}\|^2) < E^*$  and component_usage_oscillation
28: end for
29: return best

```

---

## 4 EXPERIMENT

### 4.1 SYNTHESIZED MIXED COMPONENT DATASET

Real chemical spectra seldom reveal their pure constituents or concentrations, so we construct a benchmark entirely in silico (see Algorithm. 2 for the exact sampling routine). Each spectrum lives in  $\mathbb{R}^{512}$ , mirroring the resolution of common chemical instruments. In the experiment, a pool of  $N$  non-negative basis spectra are produced by sampling an orthonormal matrix and applying an element-wise absolute value, yielding mutually distinct yet chemically plausible components. For every mixture, the active component count  $k$  is drawn uniformly from  $\{K_{\min}, \dots, K_{\text{high}}\}$  with  $K_{\min} = 1$  and  $K_{\text{max}} = 4$ , a range that reflects the limited number of dominant constituents typically encountered in laboratory samples. Concentrations are sampled uniformly from  $[1, 10)$ , ensuring that individual component signals remain on a comparable numerical scale and preventing any single component from dominating the mixture. The noiseless signal arises from summing these weighted components, after which zero-mean Gaussian noise is injected to reach a target signal-to-noise ratio (SNR), thereby emulating instrument noise. This procedure generates spectra consistent with chemical intuition while preserving ground-truth components for quantitative evaluation of EB-gMCR. Dataset size was fixed to four and eight times the component count to evaluate; the study examined  $N \in \{16, 32, 48, 64, 128, 160, 192, 224, 256\}$ , yielding between 64 ( $4N, N = 16$ ) and 2048 ( $8N, N = 256$ ) spectra per dataset and ensuring that every component appears in reasonable frequency. Five independent datasets were generated for each  $N$ , and all reported results quote the mean estimated component number together with its standard deviation across these replicates. All experiments were executed on a server running Ubuntu 24.04 LTS and equipped with two NVIDIA RTX A6000 GPUs (NVIDIA, Santa Clara, CA, USA).

---

#### Algorithm 2 Mixed Data Sampling Process to Construct a Synthesized Dataset

---

**Input:** Candidate component matrix  $S \in \mathbb{R}^{N \times d}$ , number of mixed samples  $M$ , sampling range of component count in each mixture  $K \in [K_{\min}, K_{\text{high}}]$ , concentration range for each selected component  $c \in [c_{\text{low}}, c_{\text{high}}]$

**Output:** Mixed synthesized data  $X^d$

```

1: for  $i = 1$  to  $M$  do
2:   Sample the number of components:  $k \sim \mathcal{U}\{K_{\min}, K_{\text{high}}\}$ 
3:   Randomly select a set of  $k$  component indices  $J_i \subset \{1, 2, \dots, N\}$ 
4:   for each  $j \in J_i$  do
5:     Sample concentration  $c_j \sim \mathcal{U}(c_{\text{low}}, c_{\text{high}})$ 
6:   end for
7:   Compute the mixed signal:

$$X_i = \sum_{j \in J_i} c_j \cdot S_{j,:}, \quad \text{where } S_{j,:} \text{ is the } j\text{-th component}$$

8:   if SNR (dB) is specified then
9:     Compute  $\sigma^2$  from  $\|X_i\|_2^2$  and SNR (dB)
10:    Add  $\varepsilon_i \sim \mathcal{N}(0, \sigma^2 I)$  to  $X_i$ 
11:   end if
12: end for
13: return the matrix  $X = [X_1, X_2, \dots, X_M] \in \mathbb{R}^{M \times d}$ 

```

---

### 4.2 MCR RECONSTRUCTION PERFORMANCE AND COMPONENT RETRIEVAL

To our knowledge, EB-gMCR is the first end-to-end multivariate curve resolution method that simultaneously determines the number of spectral components and resolves them, all without human input. Fig. 3 summarizes EB-gMCR’s retrieval accuracy on synthetic datasets under two sample sizes ( $4N$  and  $8N$ ) and two noise levels (SNR = 20 dB and 30 dB). At 20 dB (Fig. 3a), checkpoints chosen from the  $R^2$  bands  $[0.97, 0.975)$ ,  $[0.975, 0.98)$ , and  $[0.98, 0.985)$  yield mean component-count errors of 4.4, 9.4, and 30.7, respectively, for  $N = 256$ , corresponding to an average deviation of 5.8% from the ground truth. Raising the SNR to 30 dB (Fig. 3b) and selecting the  $[0.99, 0.995)$  band lowers the mean error to 7.2 components (2.8% deviation). With a larger sample size ( $8N$ )



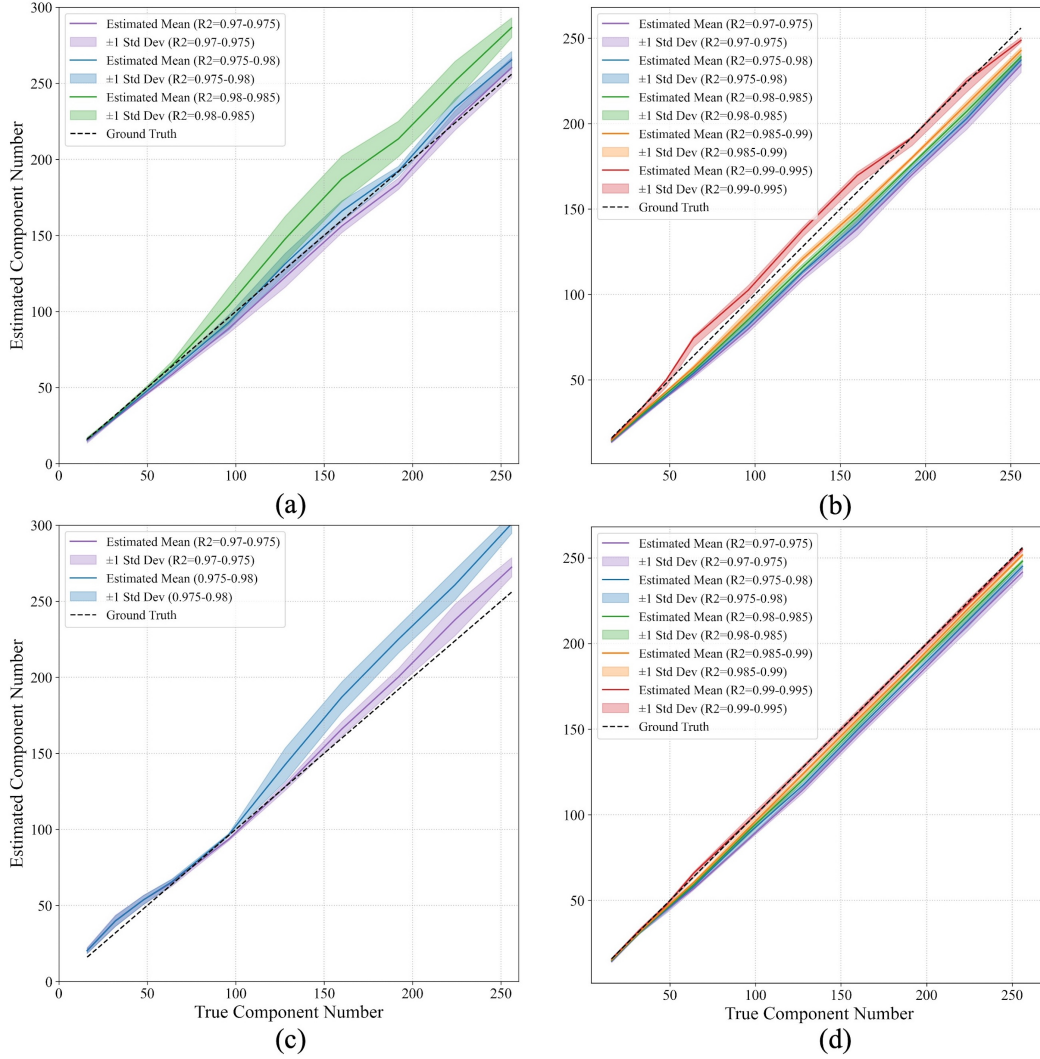


Figure 3: EB-gMCR component recovery on synthetic mixtures. Estimated vs. true component counts for five replicate datasets: solid curves, means; shaded ribbons,  $\pm 1$  SD; colors,  $R^2$  checkpoint bands (see legend). Black dashed line marks perfect agreement. Panels: (a)  $4N$ , 20 dB; (b)  $4N$ , 30 dB; (c)  $8N$ , 20 dB; (d)  $8N$ , 30 dB.

at 20 dB (Fig. 3c), the solver reports mean errors of 16.4 and 45 components in the  $[0.97, 0.975]$  and  $[0.975, 0.98]$  bands, respectively—about 11.9% deviation. Under the same sample size at 30 dB (Fig. 3d), the  $[0.99, 0.995]$  band achieves a mean error of 1.0 component (0.4% deviation). Table A.1 lists the detailed values, showing close agreement with the ground-truth component numbers across the full range (16–256), with an average spread of only 1.16 standard deviations. These results suggest a consistent trend: higher noise or fewer samples lead the solver to use more components for reconstruction, while lower noise allows nearly exact component recovery. Larger datasets also accelerate convergence; for example, the  $8N/256$ -component runs auto-stopped in approximately 2 A6000 GPU-hours, compared to 3–4 A6000 GPU-hours for the  $4N$  sets. Overall, EB-gMCR demonstrates strong potential for efficient analysis of highly mixed spectra at scale.

To enable a level comparison, every baseline was fitted with the same automatic component-search routine (Algorithm. 3). The baselines: non-negative matrix factorization (NMF) (Lee & Seung, 1999), sparse-NMF (Hoyer, 2004), Bayesian NMF (Schmidt et al., 2009), independent component analysis (ICA) (Comon, 1994), and MCR-ALS (Tauler et al., 1995) were each run 100 times on

Table 1: Comparison of EB-gMCR with five baseline solvers on 4N synthetic mixtures.

Components	Method	20dB (success $R^2 \geq 0.98$ )			30dB (success $R^2 \geq 0.99$ )		
		Succ.	$R^2$	EC	Succ.	$R^2$	EC
16	NMF	0.33	0.978±0.002	18.0±1.1	1.00	0.995±0.002	17.0±1.4
	Sparse-NMF	0.00	0.761±0.034	13.7±2.0	0.00	0.776±0.031	13.4±1.9
	Bayes-NMF	0.18	0.978±0.002	18.3±0.9	1.00	<b>0.996±0.002</b>	<b>17.6±1.4</b>
	ICA	0.00	0.106±0.172	14.7±1.9	0.00	0.079±0.199	13.8±1.4
	MCR-ALS	0.80	0.981±0.003	16.4±0.9	0.92	0.994±0.008	16.1±1.4
	EB-gMCR	-	<b>0.983±0.001</b>	<b>16.2±1.1</b>	-	0.993±0.002	15.4±0.5
32	NMF	0.01	0.976±0.002	36.4±1.6	1.00	0.992±0.001	32.7±1.2
	Sparse-NMF	0.00	0.580±0.034	25.5±1.8	0.00	0.596±0.034	25.4±1.5
	Bayes-NMF	0.08	0.978±0.002	37.3±1.3	1.00	<b>0.993±0.002</b>	<b>33.1±2.1</b>
	ICA	0.00	0.230±0.123	30.4±3.5	0.00	0.131±0.188	29.1±2.9
	MCR-ALS	0.12	0.956±0.048	29.5±2.8	0.52	0.986±0.015	30.3±2.1
	EB-gMCR	-	<b>0.982±0.001</b>	<b>31.4±0.9</b>	-	<b>0.992±0.001</b>	<b>31.4±2.2</b>
48	NMF	0.00	0.972±0.003	55.8±1.6	0.83	0.991±0.001	53.9±2.7
	Sparse-NMF	0.00	0.524±0.019	38.8±2.2	0.00	0.536±0.019	38.9±3.0
	Bayes-NMF	0.03	0.977±0.002	56.2±1.4	1.00	<b>0.992±0.001</b>	<b>49.5±1.8</b>
	ICA	0.00	0.200±0.141	47.8±5.9	0.00	0.126±0.180	43.8±3.6
	MCR-ALS	0.00	0.870±0.139	41.5±3.7	0.11	0.923±0.108	42.1±3.2
	EB-gMCR	-	<b>0.981±0.001</b>	<b>48.0±1.2</b>	-	0.992±0.001	50.0±4.2
64	NMF	0.00	0.967±0.003	74.7±2.0	0.09	0.987±0.002	74.4±2.3
	Sparse-NMF	0.00	0.509±0.019	51.0±0.0	0.00	0.518±0.018	51.1±0.6
	Bayes-NMF	0.00	0.976±0.002	74.9±1.8	1.00	<b>0.992±0.001</b>	<b>67.9±2.3</b>
	ICA	0.00	0.215±0.114	63.3±8.3	0.00	0.172±0.143	58.5±4.7
	MCR-ALS	0.00	0.770±0.226	54.2±4.1	0.00	0.876±0.183	56.5±4.9
	EB-gMCR	-	<b>0.981±0.001</b>	<b>64.8±2.6</b>	-	0.991±0.001	74.4±5.0
96	NMF	0.00	0.955±0.004	113.3±2.9	0.00	0.977±0.003	113.7±2.4
	Sparse-NMF	0.00	0.504±0.015	76.3±1.6	0.00	0.515±0.015	76.1±1.0
	Bayes-NMF	0.00	0.974±0.002	114.2±1.9	1.00	0.991±0.001	108.0±3.8
	ICA	0.00	0.245±0.077	96.0±12.0	0.00	0.194±0.100	89.5±7.8
	MCR-ALS	0.00	0.782±0.237	86.4±6.9	0.00	0.882±0.041	85.9±6.2
	EB-gMCR	-	<b>0.981±0.001</b>	<b>103.8±12.0</b>	-	<b>0.991±0.000</b>	<b>102.4±4.8</b>
128	NMF	0.00	0.938±0.005	152.0±2.2	0.00	0.962±0.006	151.4±3.0
	Sparse-NMF	0.00	0.501±0.011	102.0±0.0	0.00	0.513±0.014	102.0±0.0
	Bayes-NMF	0.00	0.970±0.002	152.0±2.2	0.66	0.990±0.001	150.7±3.5
	ICA	0.00	0.275±0.065	129.3±13.7	0.00	0.235±0.085	120.0±9.9
	MCR-ALS	0.00	0.703±0.020	116.6±8.8	0.00	0.763±0.035	118.3±7.4
	EB-gMCR	-	<b>0.981±0.000</b>	<b>147.8±14.9</b>	-	<b>0.991±0.000</b>	<b>137.6±3.8</b>
160	NMF	0.00	0.923±0.005	191.2±2.7	0.00	0.945±0.005	190.8±2.9
	Sparse-NMF	0.00	0.500±0.012	128.0±0.0	0.00	0.513±0.011	128.0±0.0
	Bayes-NMF	0.00	0.967±0.002	191.4±2.2	0.18	0.988±0.002	191.3±2.3
	ICA	0.00	0.309±0.050	151.4±17.0	0.00	0.270±0.068	146.3±11.6
	MCR-ALS	0.00	0.445±0.055	140.0±10.9	0.00	0.480±0.080	142.6±10.9
	EB-gMCR	-	<b>0.979±0.002</b>	<b>187.2±15.1</b>	-	<b>0.991±0.001</b>	<b>169.6±5.3</b>

4N synthetic sets containing 16–160 components. Table 1 lists (i) the mean estimated component count (EC), (ii) the mean reconstruction  $R^2$ , and (iii) a success rate defined as the fraction of runs that reached an  $R^2$  no lower than EB-gMCR’s own threshold (0.98 at 20 dB, 0.99 at 30 dB). At 20 dB, the classical solvers match EB-gMCR up to 32 components; beyond that point their accuracy declines, and even the strongest baseline (Bayesian NMF) starts to require noticeably more components. In the lighter-noise regime (30 dB) the baselines hold parity until about 64 components, after which EB-gMCR delivers higher  $R^2$  with fewer components. Thus, while a conventional method may suffice for small, low-noise problems, EB-gMCR scales more gracefully as the expected component count and noise level rise. The comparison presently stops at 160 components, because the rank-sweep dominates the cost beyond that point. On a 24-thread Intel i9-14900K, a single sweep across the nine candidate ranks for a 256-component, 4N dataset already requires roughly three hours when any of the five benchmark methods is driven at full CPU load. Expanding the grid or repeating the sweep for even larger ranks would multiply that wall-time until the study becomes infeasible. Moreover, Algorithm B.1 assumes the true rank is known, an assumption that fails for real data. An adaptive search similar to the strategy proposed by (Smith et al., 2019) can discover the rank automatically, yet its runtime would grow dramatically once the target surpasses about one hundred components.

Table 2: Ablation study for EB-gMCR (256 latent components). Each row removes one mechanism from the standard solver and reports the resulting reconstruction  $R^2$ , estimated component count (EC), and mean wall-time (hours  $\pm$  SD, three runs) on a 24-thread Intel i9-14900K. Results appear for two noise levels (20 dB, 30 dB) and two sample counts ( $4N = 1024$  and  $8N = 2048$  mixed spectra).

Solver	Noise=20dB			Noise=30dB		
	$R^2$	EC	Time (hr.)	$R^2$	EC	Time (hr.)
<b>Data size = 4N (1024 mixed samples)</b>						
EB-gMCR	0.978 $\pm$ 0.003	278.0 $\pm$ 13.4	3.6 $\pm$ 0.8	0.990 $\pm$ 0.000	248.8 $\pm$ 1.1	3.3 $\pm$ 0.6
w/o SGLD	0.980 $\pm$ 0.001	292.0 $\pm$ 8.2	4.7 $\pm$ 0.3	0.990 $\pm$ 0.000	257.8 $\pm$ 6.2	2.9 $\pm$ 0.3
w/o $C(X_o)$	0.980 $\pm$ 0.001	284.6 $\pm$ 13.4	4.1 $\pm$ 0.3	0.995 $\pm$ 0.000	268.2 $\pm$ 4.5	4.1 $\pm$ 0.3
w/o $\ E_{f_e}\ _2^2$	0.979 $\pm$ 0.002	282.0 $\pm$ 20.3	6.1 $\pm$ 0.2	0.990 $\pm$ 0.000	251.8 $\pm$ 3.4	6.0 $\pm$ 0.4
w/o $\mathcal{R}(X_o)$	0.980 $\pm$ 0.000	292.2 $\pm$ 13.0	3.8 $\pm$ 0.6	0.990 $\pm$ 0.000	249.0 $\pm$ 1.6	4.5 $\pm$ 0.7
<b>Data size = 8N (2048 mixed samples)</b>						
EB-gMCR	0.975 $\pm$ 0.000	301.0 $\pm$ 6.4	2.0 $\pm$ 0.2	0.991 $\pm$ 0.001	255.0 $\pm$ 1.4	2.1 $\pm$ 0.2
w/o SGLD	0.976 $\pm$ 0.002	323.8 $\pm$ 41.2	2.5 $\pm$ 0.3	0.991 $\pm$ 0.000	255.8 $\pm$ 0.4	2.0 $\pm$ 0.3
w/o $C(X_o)$	0.975 $\pm$ 0.000	318.6 $\pm$ 32.2	2.2 $\pm$ 0.1	0.993 $\pm$ 0.002	298.2 $\pm$ 29.3	2.4 $\pm$ 0.2
w/o $\ E_{f_e}\ _2^2$	0.975 $\pm$ 0.000	290.4 $\pm$ 11.9	12.1 $\pm$ 0.1	0.979 $\pm$ 0.000	255.6 $\pm$ 0.5	12.2 $\pm$ 0.1
w/o $\mathcal{R}(X_o)$	0.975 $\pm$ 0.002	305.4 $\pm$ 6.4	2.5 $\pm$ 0.5	0.991 $\pm$ 0.000	254.8 $\pm$ 0.8	2.2 $\pm$ 0.1

EB-gMCR turns component number estimation into part of the optimization itself. An EB-select variational gate learns during training to switch individual components on or off, converging to a compact subset that recurs across independent draws and keeps the component-count error within 5%. Even with 256 latent sources the solver maintains reconstruction  $R^2$  above 0.98—a scale at which classical MCR routines lose stability. By combining reliable energy-based optimization framework and GPU-level throughput measured in hours rather than days, EB-gMCR extends MCR into the hundred-component regime without manual tuning.

#### 4.3 ABLATION STUDY

EB-gMCR solves the gMCR task by combining three ingredients: (1) EB-select – a variational gate that keeps only the useful components; (2) Energy-based optimization – a loss made of the main MSE term plus four auxiliaries for sparsity and diversity (SGLD exploration, the component count penalty  $C(X_o)$ , the minimum selection energy term  $\|E_{f_e}\|_2^2$ , and the HSIC redundancy penalty  $\mathcal{R}(X_o)$ ; (3) Checkpointing – a simple rule that records the best parameter state during training. To see how each part matters, we remove one mechanism at a time and rerun the solver on the most demanding case—256 latent components—under two noise levels (20 dB and 30 dB) and two sample counts (1024 and 2048). Table 2 reports the reconstruction  $R^2$ , the estimated component count (EC), and the wall-time until auto-stop. A fixed-rank variant was not included because using 1024 unconstrained components reduces to generative variant of NMF-like optimization in the synthetic dataset and offers no insight into rank-selection dynamics.

The main MSE loss is sufficient for accurate reconstruction. All variants maintain  $R^2 \geq 0.97$  at 20 dB and  $R^2 \geq 0.99$  at 30 dB, indicating that the auxiliary terms primarily enhance efficiency rather than fit quality. The SGLD term matters in heavy noise. Removing SGLD speeds the solver and even sharpens the EC under 30 dB, yet it inflates EC and runtime under 20 dB. Extra gradient noise therefore helps the gate avoid noisy local minima. The component-count penalty prevents over-use. Dropping  $C(X_o)$  raises  $R^2$  only 0.002–0.003 but adds 10–20 extra components, confirming its role as a sparsity brake that curbs overfitting when noise is strong. The minimum-energy term controls convergence. Without  $\|E_{f_e}\|_2^2$  the solver never meets its selection-energy threshold and simply times out at the 100,000 epochs limit, more than doubling wall-time. The HSIC penalty has little effect here. Its weight is  $10^{-10}$  and the synthetic spectra were generated to be nearly orthogonal; real mixtures with correlated sources are expected to benefit more. Overall, the full EB-gMCR configuration remains the only variant that keeps component usage tight and runtime low across both noise regimes, underlining its suitability for large, noisy chemical datasets.

An intriguing side observation is that, even after the component-count penalty is removed, EB-select still prunes roughly 256 active components out of 1024 candidates without SGLD assistance—essentially performing a straight-through hard selection. This intrinsic sparsity hints that

the EB-select could be transferable to other discrete-routing tasks, such as vector quantization or expert selection in mixture-of-experts transformers, although we leave a full exploration of that idea to future work.

#### 4.4 POTENTIAL OF EB-GMCR FRAMEWORK

The experiments above use the classic MCR setting, where traditional solvers still compete with EB-gMCR at modest data sizes and component counts. EB-gMCR’s real value emerges when those limits expand. In mass spectral analysis, for example, thousands of library patterns can be inserted directly as fixed components (fix  $f_s$  in the training); the network only needs to learn the EB-select gate and the concentration predictor. The solver’s accuracy actually improves as the number of spectra grows, turning what is usually a data volume bottleneck into an advantage. These features suggest that EB-gMCR could evolve into a general-purpose decomposer for analytical chemistry signals. The framework also invites easy extensions. Any physical constraint (linear or nonlinear) can enter the forward model with minimal code changes. If an exponential mixing rule replaces a linear one, only the forward pass requires modification; the loss terms remain intact because they depend on the energies of component selection decision and the RKHS-based duplication penalty, not on the specific mixing law or the location of components in feature space. Consequently, EB-gMCR can adapt to non-chemical mixtures wherever fixed, reusable basis patterns exist.

## 5 CONCLUSION

Multivariate curve resolution has been re-cast as generative multivariate curve resolution (gMCR), a formulation that treats mixing as an explicit data generation process. A single generative graphical model covers mixtures that draw on just a few library patterns as well as those that draw on the entire library, giving gMCR one unified framework for both routine and extreme signal unmixing problems. The accompanying solver, is driven by EB-select, a differentiable hard selection gate that learns the active subset of components in a single pass. On synthetic mixtures, the solver kept reconstruction  $R^2$  above 0.98 and chose a component count within 5% of the ground truth at ranks up to 256. Under the largest data size tested (8N spectra) and light noise (30 dB), the retrieved component count matched the ground truth exactly. Runtime decreased as the number of spectra increased, turning a long-standing data volume bottleneck into an advantage. Classical factorization baselines lost accuracy or stalled beyond 64 components and showed super-linear scaling with rank. These findings demonstrate that a generative perspective combined with a learned selection gate pushes signal unmixing into the hundred-component regime and accommodates large datasets—an operating range previously inaccessible to traditional MCR tools. By enabling accurate, hands free decomposition at scale, the framework opens a practical path toward high throughput, library-driven spectral analysis in routine analytical chemistry workflows and offers a transferable blueprint for other ML domains that require hard selection (decision) modeling.

**Author’s note.** Results to date are synthetic; real-world benchmarks are in progress and will appear in a forthcoming revision.

#### AUTHOR CONTRIBUTIONS

All conceptual development, experimental design, and implementation were carried out by the first author. The second author is listed per lab authorship policy.

## REFERENCES

- A. Barcaru, H. G. Mol, M. Tienstra, and G. Vivó-Truyols. Bayesian approach to peak deconvolution and library search for high resolution gas chromatography–mass spectrometry. *Analytica Chimica Acta*, 983:76–90, 2017.
- Pierre Comon. Independent component analysis, a new concept? *Signal Processing*, 36(3):287–314, 1994.
- A. de Juan and R. Tauler. Multivariate curve resolution: 50 years addressing the mixture analysis problem—a review. *Analytica Chimica Acta*, 1145:59–78, 2021.

- Arthur Gretton, Ralf Herbrich, Alex Smola, Olivier Bousquet, Bernhard Schölkopf, and Aapo Hyvärinen. Kernel methods for measuring independence. *Journal of Machine Learning Research*, 6(12), 2005.
- Richard A. Harshman. Parafac2: Mathematical and technical notes. Technical Report 22, UCLA Working Papers in Phonetics, 1972.
- A. Heinecke, L. Ye, M. De Iorio, and T. Ebbels. Bayesian deconvolution and quantification of metabolites from j-resolved nmr spectroscopy. *Bayesian Analysis*, 16(2):425–458, 2021.
- Patrik O. Hoyer. Non-negative matrix factorization with sparseness constraints. *Journal of Machine Learning Research*, 5:1457–1469, 2004.
- Eric Jang, Shixiang Gu, and Ben Poole. Categorical reparameterization with gumbel-softmax. *arXiv preprint arXiv:1611.01144*, 2016.
- H. R. Keller and D. L. Massart. Evolving factor analysis for the resolution of overlapping chromatographic peaks. *Analytical Chemistry*, 63(20):2343–2347, 1991.
- W. H. Lawton and E. A. Sylvestre. Self modeling curve resolution. *Technometrics*, 13(3):617–633, 1971.
- Yann LeCun, Sumit Chopra, Raia Hadsell, M Ranzato, Fugie Huang, et al. A tutorial on energy-based learning. *Predicting structured data*, 1(0), 2006.
- Daniel D. Lee and H. Sebastian Seung. Learning the parts of objects by non-negative matrix factorization. *Nature*, 401(6755):788–791, 1999.
- Ilya Loshchilov and Frank Hutter. Decoupled weight decay regularization. *arXiv preprint arXiv:1711.05101*, 2017.
- Chris J. Maddison, Andriy Mnih, and Yee Whye Teh. The concrete distribution: A continuous relaxation of discrete random variables. *arXiv preprint arXiv:1611.00712*, 2016.
- Mikkel N. Schmidt, Ole Winther, and Lars K. Hansen. Bayesian non-negative matrix factorization. In *International Conference on Independent Component Analysis and Signal Separation*, pp. 540–547. Springer, 2009.
- J. P. Smith, E. C. Holahan, F. C. Smith, V. Marrero, and K. S. Booksh. A novel multivariate curve resolution-alternating least squares (mcr-als) methodology for application in hyperspectral raman imaging analysis. *Analyst*, 144(18):5425–5438, 2019.
- R. Tauler, A. Smilde, and B. Kowalski. Selectivity, local rank, three-way data analysis and ambiguity in multivariate curve resolution. *Journal of Chemometrics*, 9(1):31–58, 1995.
- Max Welling and Yee Whye Teh. Bayesian learning via stochastic gradient langevin dynamics. In *Proceedings of the 28th International Conference on Machine Learning (ICML-11)*, pp. 681–688, 2011.

## APPENDIX

## A DETAILED RESULTS OF EB-GMCR SOLVER’S COMPONENT ESTIMATION

Table 3 lists the exact mean  $\pm 1$  SD component counts that form every point and ribbon in Figure 3. The rows cover all four dataset settings (4  $N$  and 8  $N$  samples, each at 20 dB and 30 dB noise) and group the results by the  $R^2$  checkpoint bands used for model selection. Each entry reflects the average over five independent draws, identical to those in the figure. Readers who wish to reproduce the curves, perform secondary analyses, or benchmark alternative solvers can extract the numeric values directly from this table.

Table 3: Exact numerical values underlying Fig. 3: mean  $\pm$  1 SD estimated component numbers returned by EB-gMCR for each dataset size ( $4N$ ,  $8N$ ) and noise level (20 dB, 30 dB).

<b>R<sup>2</sup> band</b>	<b>16</b>	<b>32</b>	<b>48</b>	<b>64</b>	<b>96</b>	<b>128</b>	<b>160</b>	<b>192</b>	<b>224</b>	<b>256</b>
<b>Data size = 4N (SNR = 20 dB)</b>										
0.97–0.975	15.2 $\pm$ 1.6	29.8 $\pm$ 0.4	44.4 $\pm$ 0.5	58.6 $\pm$ 1.1	88.8 $\pm$ 3.0	122.6 $\pm$ 6.5	156.2 $\pm$ 4.3	184.0 $\pm$ 3.7	225.6 $\pm$ 6.3	260.4 $\pm$ 6.6
0.975–0.98	15.8 $\pm$ 1.3	30.4 $\pm$ 0.5	46.0 $\pm$ 0.7	61.4 $\pm$ 1.3	92.8 $\pm$ 4.9	131.4 $\pm$ 6.9	166.0 $\pm$ 6.8	192.4 $\pm$ 3.0	234.0 $\pm$ 6.0	265.4 $\pm$ 5.6
0.98–0.985	16.2 $\pm$ 1.1	31.4 $\pm$ 0.9	48.0 $\pm$ 1.2	64.8 $\pm$ 2.6	103.8 $\pm$ 12.0	147.8 $\pm$ 14.9	187.2 $\pm$ 15.1	213.5 $\pm$ 11.6	251.5 $\pm$ 13.0	286.7 $\pm$ 6.4
<b>Data size = 4N (SNR = 30 dB)</b>										
0.97–0.975	13.6 $\pm$ 0.5	27.0 $\pm$ 0.7	39.8 $\pm$ 0.4	52.4 $\pm$ 1.1	79.6 $\pm$ 2.1	110.2 $\pm$ 1.9	138.6 $\pm$ 4.3	170.0 $\pm$ 2.0	200.4 $\pm$ 3.8	234.4 $\pm$ 4.4
0.975–0.98	14.2 $\pm$ 0.4	27.6 $\pm$ 0.5	40.4 $\pm$ 0.5	53.8 $\pm$ 0.8	82.0 $\pm$ 2.4	113.2 $\pm$ 0.8	141.2 $\pm$ 3.0	173.2 $\pm$ 1.8	202.8 $\pm$ 2.5	237.2 $\pm$ 2.6
0.98–0.985	14.4 $\pm$ 0.5	28.2 $\pm$ 0.8	41.8 $\pm$ 0.4	55.2 $\pm$ 1.1	85.2 $\pm$ 2.8	116.0 $\pm$ 1.9	145.2 $\pm$ 2.2	176.2 $\pm$ 0.8	207.0 $\pm$ 2.0	239.2 $\pm$ 1.9
0.985–0.99	14.8 $\pm$ 0.4	29.2 $\pm$ 0.8	43.2 $\pm$ 0.4	57.2 $\pm$ 1.1	88.4 $\pm$ 1.9	120.8 $\pm$ 1.1	149.2 $\pm$ 1.6	180.0 $\pm$ 1.0	211.2 $\pm$ 1.5	242.8 $\pm$ 1.3
0.99–0.995	15.4 $\pm$ 0.5	31.4 $\pm$ 2.2	50.0 $\pm$ 4.2	74.4 $\pm$ 5.0	102.4 $\pm$ 4.8	137.6 $\pm$ 3.8	169.6 $\pm$ 5.3	191.8 $\pm$ 4.6	224.8 $\pm$ 6.3	248.8 $\pm$ 1.1
<b>Data size = 8N (SNR = 20 dB)</b>										
0.97–0.975	20.4 $\pm$ 1.9	40.0 $\pm$ 3.7	53.8 $\pm$ 2.9	65.0 $\pm$ 2.2	93.4 $\pm$ 0.9	128.2 $\pm$ 2.5	166.0 $\pm$ 4.8	200.2 $\pm$ 5.5	237.8 $\pm$ 10.4	272.4 $\pm$ 6.3
0.975–0.98	20.2 $\pm$ 1.6	39.8 $\pm$ 4.4	53.8 $\pm$ 2.9	65.6 $\pm$ 1.9	96.4 $\pm$ 0.9	142.6 $\pm$ 11.0	187.0 $\pm$ 10.0	225.0 $\pm$ 9.0	260.8 $\pm$ 9.9	301.0 $\pm$ 6.4
<b>Data size = 8N (SNR = 30 dB)</b>										
0.97–0.975	14.4 $\pm$ 0.5	31.2 $\pm$ 0.8	44.4 $\pm$ 1.7	57.0 $\pm$ 0.7	85.8 $\pm$ 0.8	114.8 $\pm$ 1.8	147.2 $\pm$ 1.9	178.4 $\pm$ 1.7	210.4 $\pm$ 0.7	241.6 $\pm$ 2.3
0.975–0.98	14.8 $\pm$ 0.4	31.2 $\pm$ 0.8	44.8 $\pm$ 1.3	58.2 $\pm$ 0.6	89.2 $\pm$ 2.5	117.4 $\pm$ 1.5	150.0 $\pm$ 1.9	181.6 $\pm$ 1.1	213.2 $\pm$ 3.3	245.0 $\pm$ 1.1
0.98–0.985	15.0 $\pm$ 0.4	31.2 $\pm$ 0.8	45.4 $\pm$ 0.9	59.2 $\pm$ 0.7	90.6 $\pm$ 2.2	120.6 $\pm$ 1.1	153.0 $\pm$ 1.9	185.0 $\pm$ 1.4	216.4 $\pm$ 2.3	248.0 $\pm$ 1.1
0.985–0.99	15.4 $\pm$ 0.5	31.2 $\pm$ 0.5	46.0 $\pm$ 0.7	61.0 $\pm$ 0.5	92.2 $\pm$ 1.6	124.0 $\pm$ 1.6	156.0 $\pm$ 1.2	187.2 $\pm$ 1.1	220.0 $\pm$ 1.3	251.6 $\pm$ 0.5
0.99–0.995	16.0 $\pm$ 0.5	32.4 $\pm$ 0.5	47.4 $\pm$ 0.5	66.0 $\pm$ 0.5	96.2 $\pm$ 0.8	128.0 $\pm$ 1.6	159.6 $\pm$ 1.1	191.8 $\pm$ 0.4	223.0 $\pm$ 0.8	255.0 $\pm$ 1.4

## B BENCHMARK SEARCH WRAPPER FOR BASELINE MCR SOLVERS

To place each traditional MCR algorithm on equal footing with EB-gMCR, we wrap every solver in a simple rank search helper (Algorithm. 3). Because the ground-truth component count  $C^*$  is known for the synthetic datasets, the wrapper probes a small band around that value and returns the best reconstruction it achieves. If the true rank were unknown—as in a real experiment—the baseline would need to extend the probe range and its runtime would grow unpredictably; for clarity we restrict the search to the nine ratios listed in  $S$ .

---

### Algorithm 3 Rank-search proxy for baseline MCR methods

---

**Input:** Observed data  $D_o$ , MCR solver initialized with  $C$  components  $f(\cdot, C)$ , target reconstruction  $R^2 \hat{R}$ , True component number  $C^*$ , Searching ratios  $S = \{0.80, 0.85, 0.90, 0.95, 1.00, 1.05, 1.10, 1.15, 1.20\}$

**Output:** Success  $\in \{0, 1\}$ ,  $R_{\text{best}}^2$ ,  $C_{\text{sel}}$

```

1:  $R_{\text{best}}^2 \leftarrow -\infty$ ,  $C_{\text{sel}} \leftarrow \text{None}$ 
2: for  $s$  in  $S$  do
3:    $C_{\text{try}} \leftarrow \lfloor s \cdot C^* \rfloor$ 
4:    $R^2 \leftarrow f(D_o, C_{\text{try}})$  ▷ run solver and compute  $R^2$ 
5:   if  $R^2 \geq R_{\text{best}}^2$  then
6:      $R_{\text{best}}^2 \leftarrow R^2$ 
7:      $C_{\text{sel}} \leftarrow C_{\text{try}}$ 
8:   end if
9: end for
10: success  $\leftarrow 1$  if  $R_{\text{best}}^2 \geq \hat{R}$  else 0
11: return success,  $R_{\text{best}}^2$ ,  $C_{\text{sel}}$ 
```

---